ISTANBUL TECHNICAL UNIVERSITY ★ GRADUATE SCHOOL OF SCIENCE ENGINEERING AND TECHNOLOGY

IMAGING OF MULTIPLE SLICES WITH SINGLE LATERAL SCAN

M.Sc. THESIS

Miyase TEKPINAR

Department of Electronics and Communication Engineering

Telecommunication Engineering Programme

JUNE 2020

ISTANBUL TECHNICAL UNIVERSITY ★ GRADUATE SCHOOL OF SCIENCE ENGINEERING AND TECHNOLOGY

IMAGING OF MULTIPLE SLICES WITH SINGLE LATERAL SCAN

M.Sc. THESIS

Miyase TEKPINAR
(504171320)

Department of Electronics and Communication Engineering

Telecommunication Engineering Programme

Thesis Advisor: Assoc. Prof. Dr. Onur FERHANOĞLU

JUNE 2020

İSTANBUL TEKNİK ÜNİVERSİTESİ ★ FEN BİLİMLERİ ENSTİTÜSÜ

TEK BİR DÜZLEMSEL TARAMA İLE BİR ÇOK KATMANIN GÖRÜNTÜLENMESİ

YÜKSEK LİSANS TEZİ

Miyase TEKPINAR
(504171320)

Elektronik ve Haberleşme Mühendisliği Anabilim Dalı

Telekomünikasyon Mühendisliği Programı

Tez Danışmanı: Assoc. Prof. Dr. Onur FERHANOĞLU

HAZİRAN 2020

Miyase TEKPINAR, a M.Sc. student of ITU Graduate School of Science Engineering and Technology 504171320 successfully defended the thesis entitled "IMAGING OF MULTIPLE SLICES WITH SINGLE LATERAL SCAN", which he/she prepared after fulfilling the requirements specified in the associated legislations, before the jury whose signatures are below.

Thesis Advisor :	**Assoc. Prof. Dr. Onur FERHANOĞLU** Istanbul Technical University	.....
Jury Members :	**Assist. Prof. Ahmet Can ERTEN** Istanbul Technical University	.....
	Assist. Prof. Muhammed Fatih TOY Medipol University	.....
		.....

Date of Submission : **15 June 2020**
Date of Defense : **30 June 2020**

To my family,

FOREWORD

I would like to thank my advisor, Dr. Onur Ferhanoglu for encouraging me from the very beginning and for his guidance through the years of my master's study. I feel fortunate to have the opportunity to work in EDL which led me to a very exciting field for my future work. Also, I am very thankful to Dr. Fatih Toy for his valuable conversations and advice. Lastly, I would like to thank my family for their endless support and love.

I would like to thank my co-author Ramin KHAYATZADEH for his cooperation in performing the COMSOL simulations and for the figures in the third section.

June 2020 Miyase TEKPINAR

TABLE OF CONTENTS

Page

ABBREVIATIONS

3D	**:** 3-Dimensional
CMOS	**:** Complementary Metal-Oxide Semiconductor
FOV	**:** Field-of-View
FPS	**:** Frame Per Second
FWHM	**:** Full Width Half Maximum
MEMS	**:** Micro Electrical Mechanical Systems
NA	**:** Numerical Aperture
SMF	**:** Single Mode Fiber
MMF	**:** Multi Mode Fiber
USAF	**:** United States Air Force
FEM	**:** Finite Element Methods
DOF	**:** Depth of Field
SBR	**:** Signal to Noise Ratio
CM	**:** Confocal Microscopy
SDCM	**:** Spinning Disk Confocal Microscopy
LSCM	**:** Laser Scanning Confocal Microscopy
OCT	**:** Optical Coherence Tomography
TPM	**:** Two Photon Microscopy
TEM	**:** Transverse Electro-Magnetic
SLM	**:** Spatial Light Modulator
BS	**:** Beam Splitter
PD	**:** Photo Detector
OBJ	**:** Objective Lens

SYMBOLS

f	: frequency
λ	: wavelength
w_0	: beam waist size
z_R	: Rayleigh range
r	: radial coordinate
z	: axial coordinate
θ	: azimuth coordinate
L	: Length
W	: Width
t	: thickness
d	: diameter
k_r	: radial wavevector
k_z	: longitudinal wavevector
J_0	: zeroth-order Bessel function
E	: Young's modulus
ρ	: denstiy
μ	: micro

LIST OF TABLES

Page

LIST OF FIGURES

Page

IMAGING OF MULTIPLE SLICES WITH SINGLE LATERAL SCAN

SUMMARY

Bessel beams or so-called non-diffracting beams have received great attention from the biomedical optics community, especially in 3D imaging researches, with its long propagation distance in diffractive mediums (see section 1.1). This work presents an architecture to create higher-order Bessel-like optical beams, through off-axis coupling of light into a multimode fiber. Utilizing the aberration that is inherent in spherical surfaces, through directing the Bessel-like beam comprising multiple concentric rings onto a low-cost lens, we created multiple foci at different depths. Moreover, scanning of the optical fiber with a piezoelectric actuator in the lateral direction, we were able to acquire data from different targets located at different lateral planes, therefore proposing a faster confocal system. After coupling back into the fiber, the reflected portions of light from different targets could be spatially differentiated and directed to different photo-detection units. The proposed architecture is particularly appealing for laser scanning endoscopy applications, as it does not require additional passive or active optical components for generating Bessel beams (axicons or spatial light modulators), therefore offering both miniaturized realization and high optical transmission. We've further demonstrated the tunability of foci separation via altering fiber-coupling conditions with tilt and translation stages. Overall, the proposed scanning method has paved the way for addressing multiple slices at single lateral scan, thus offering improved speed for imaging or ablation applications.

Secondly, towards laser scanning endoscopy(LSE), a two-dimensional piezo-fiber actuator geometry is proposed to achieve three different scanning pattern with single device. Laser scanning endoscopes have been developed as a miniaturized versions of laser scanning microscopes, allowing imaging of internal organs and body cavities that are difficult to access otherwise, in a minimally invasive fashion. LSE harbors one or multiple of MEMS scanning devices, piezoelectric fiber actuators, or rotating micromotors to scan the laser spot on the desired tissue. While the scientific literature regarding LSE research has focused on a single scan pattern per presented device, by having multiple scan options, the operator of the actuator can choose between improved uniformity, high frame rate to image abrupt biological event, or circular field-of-view to better image cylindrical cavities (gastrointestinal tract, esophagus, etc.) that are cylindrical in nature. The capabilities of the device has been demonstrated through first presenting its mechanical frequency behavior, then offering an actuation scheme to achieve different scan patterns, and finally generating 256 pixel width or diameter raster, spiral, and Lissajous patterns at ≥ 20 frames per second. With further development, the presented actuator design and drive scheme could serve as a useful tool as part of a minimally invasive optomedical device in the clinic

Finally, the compact 3D imaging system utilizing both proposed methods will allow addressing multiple slices at a single lateral scan, thus offering improved speed and different scanning pattern options for endoscopic applications.

TEK BİR DÜZLEMSEL TARAMA İLE BİR ÇOK KATMANIN GÖRÜNTÜLENMESİ

ÖZET

Gaussian demetleri halen yaygın olarak görüntüleme tercih edilse de, Bessel ışınları veya kırınım yapmayan ışınlar, difraktif ortamlarda uzun yayılma mesafesi sağlaması nedeni ile biyomedikal optik camiasından, özellikle 3B görüntüleme araştırmalarında, büyük ilgi gördü (bkz. Bölüm 1.1). İdeal bir Bessel profili, optik merkez etrafında çevrelenmiş sonsuz sayıda halkasal ışın demetinden oluşur. Bu yan loblar, Bessel ışınlarına Gaussian ışınları ile başarılamayacak iki önemli avantaj kazandırır. İlk avantaj, uzatılmış odak uzaklığıdır çünkü bu yan loblar sayesinde Bessel ışını saçılmaya karşı daha dayanıklıdır. İkinci olarak, bu ışınlar kedilerini, saçılma etkisi olan engellerden sonra bir Gaussian ışığına göre daha çok yenileme kapasitesine sahiptir. Bessel beamler kullanılarak konfokal bir görüntüleme sisteminde çözünürlük arttırılabilir ya da iki foton mikroskopisinde çözünürlük korunurken odak derinliği arttırılabilir. Ancak bunların yanında, bu çevresel loblar arka plan ışığının artmasına neden olarak görüntülenen bölgenin kontrastını düşürebilir. Birkaç on yıldır araştırmacıların ilgisinin kazanan bu yeni tip ışınlardan daha iyi yararlanabilmek için bu avantajları korurken aynı zamanda nasıl konrtastın arttırılabileceğine yönelik birçok çalışma literatürde mevcuttur.

Bessel ışınları ilk olarak yakınsak bir merceğin arkasına yerleştirilen, ince dairesel bir açıklığın düzlemsel ışın demeti ile aydınlatılması sonucu elde edilmiştir. Ancak daha efektif bir yol olarak aksikon lensler ya da daha kontrollü bir method olarak uzaysal ışık modülatörleri kullanılabilir. Bunların yanında, özellikle kompakt sistemlerde kullanılmak üzere, çok modlu fiberlerde oluşan girişimden de yararlanılmıştır. Faklı açılarda ve konumlardan fiberde odaklanan ışık, halkasal profile sahip ışın demetlerinin oluşmasını sağlar ve bu yöntem kullanılarak Bessel-benzer de denilen, fiziksel Bessel ışınları üretilebilir.

Bu çalışmada ilk olarak optik eksenin dışından bir ışık hüzmesinin çok modlu bir optik fiber ile iletilmesi sonucu yüksek mertebeden Bessel benzeri optik ışınlar elde edildi. Eş-merkezli halkalar içeren Bessel ışınını düşük maliyetli bir merceğe yönlendirerek, küresel aberasyonun etkisiyle, farklı derinliklerde bir çok odak oluşturduk. Farklı derinlikteki hedeflerden yansıyan ışınlar optik fiber ile ters yönde iletildi ve farklı lateral konumlardaki foto-detektörlere düşürülerek ayırt edildi. Bu odaklar arasındaki mesafeyi ölçebilmek için ilk olarak farklı derinliklerdeki aynalardan yansıyan ışık yoğunluğunun grafiğini çizdirdik. Sistemin prensibini göstermek için iki halka kullandık ve odaklar arası açıklığın 600 μm ile 900 μm arasında değiştiğini gözlemledik. İkinci adım olarak artık USAF çözünürlük hedeflerini gözlemlediğimiz odaklara yerleştirdik. Optik fiberin lateral yönde bir piezoelektrik aktüatör ile taranmasıyla, farklı lateral düzlemlerde bulunan odaklardan veri elde edebildik. Bu arka arkaya yerleştirilmiş hedefler yansıyan ışık ile hedefler üzerindeki çizgisel desen arasındaki uyumu fotodetektöre bağlanmış çift kanallı bir osiloskop

yardımıyla gözlemledik. Her ne kadar iki halkalı bir ışık profili kullanılmış olsa da bu mimari kullanılarak daha fazla sayıda halkaya sahip çıkışlar elde etmek mümkündür. Önerilen yöntem ek bir aktif ya da pasif optik eleman gerektirmeden yüksek optik iletim sağlaması ile, gerek lazer taramalı endoskopi uygulamaları gerek görüntüleme sistemlerinin kompaktlaştırılması açısından ilgi çekicidir.

Lazer tarayan mikroskoplar, konfokal, çok-fotonlu ve/veya optik koherans tomografi ile hücresel görüntülemede kullanılırken, ışığın saçılması ve absorbe olması derin görüntülemenin önüne geçer. Bu nedenle, lazer tarayan endoskopi sistemleri, insan vücudunda ulaşması zor bölgelere, minimum müdahale ile ulaşabilmek için geliştirilmiştir. Bu yöntemde, MEMS cihazlar, piezo-fiber actüatörler ya da mikromotorlar tarayıcı olarak kullanılmıştır. Tüm bu cihazlar genel olarak raster, spiral ya da lissajous olarak adlandırılan tarama desenlerinden birinden yararlanır.

Spiral tarama çoğunlukla silindirik piezo-elektrik materyal ile oluşturulan sistemlerde raster taramadan daha çok tercih edilir. Optik fiberin silindirik geometrisi birbirine ortogonal olan iki yönde de aynı mekanik rezonans frekansı ile sonuçlanır ve 90-derece faz farklı ile sürülen elektrotlar, genlik modülasyonu ile beraber spiral bir patern oluşturur. Dairesel bir görüş alanı sağlaması nedeniyle, bu yöntem özellikle vücutta silindirik boşlukların görüntülenmesinde iyi bir tercih olabilirken, ışık yoğunluğu eş dağılımlı değildir ve ortada daha parlaktır. Raster tarama ise eşdağılımlı bir ışık yoğunlupu sağlarken, yavaş eksen için yüksek voltajlı ve geniş bantta sinyal gerektirir. Son olarak Lissajous tarama kullanılarak, bir kare için gereken sürede daha hızlı görüntü oluşturulabilir. Ancak bu yöntemdeki dezavantaj ise daha az aydınlatılmış ve çarpık dağılımlı bir patern oluşmasıdır. Bilimsel literatür şimdiye kadar bir tarayıcı tasarımı için bir tarama modeli üzerinde odaklanmış olsa da bir tek tarayıcı cihaz ile birçok görüntüleme deseninden faydalanmak önemlidir. Böylece tek bir endoskopi cihazı ile, en kirik olan faktöre göre, yüksek kare hızı, eş yoğunlukta bir desen ya da dairesel bir desen tercih edilebilir veya diğerine geçiş yapılabilir.

İlk çalışmaya ek olarak, iki boyutlu bir piezo-fiber actüatör geometrisi kullanılarak üç farklı tarama modeli aynı cihazla elde edildi. Faklı opsiyonların varlığı sayesinde operatör, görüntülenmek istenen bölgenin özelliğine göre istediği bir modeli seçebilir: geliştirilmiş düzgünlükte bir tarama, yüksek görüntüleme hızı ya da silindirik bölgeler (gastrointestinal sistem, yemek borusu) için dairesel görüş alanı. Birbirine dik yerleştirilmiş farklı uzunlukta iki piezoelektrik malzeme ve ucunda uzatılmış bir tek modlu optik fiberden oluşan cihazın mekanik frekans davranışını ve desenleri incelemek için fiberden çıkan ışık on kat büyütülerek önce USAF çözünürlük hedefine sonra da CMOS kameraya yönlendirildi. Frekans cevabı oluşturmak için geniş bir frekans aralığı boyunca, her bir frekans değeri için kameradaki tarama uzunluğu kaydedildi. Deneysel olarak elde edilen veri ile COMSOL programı kullanılarak elde edilen sonuçların birbirine çok yakın olduğu gözlemlendi. Simülasyon sonuçlarından taramalarda kullanılmak üzere optik frekansın iki doğrultudaki temel modları ile yatay eksendeki piezonun temel ve üçüncü modları seçildi. Yatay materyalin ve fiberin uzunluğu elektro-mekanik açıdan sistemin verimini arttıracak şekilde seçimler yapıldı. Tüm tarama desenleri 256 pixel genişlikte ya da çapta bir alan taranarak gösterilmiştir. Lissajous modeli ise saniyede 20 kareden fazla bir hıza ulaşabilmiştir. Ayrıca bu model için farklı kare hızları için desendeki ışık doluluk oranı analizi, iki farklı çözünürlük değeri için yapılarak 20 fps için % 93 e kadar dolu bir tarama elde edilebildiği gözlemlenmiştir.

Son olarak, her iki yöntemi bir arada kullanarak, tek bir yanal taramada birden fazla derinliğe ulaşan, yüksek hız ve farklı tarama modeli seçenekleri sunan, kompakt bir 3B görüntüleme sistemi geliştirilebilir. Önerilen tasarım, bir minimal-invazif opto-mekanik sistem olarak kliniklerde kullanılabilir.

1. INTRODUCTION

Towards 3D imaging of biological specimens, different imaging modalities including confocal microscopy [3, 4], optical coherence tomography [5], and multi-photon imaging [6] have been widely used as well as various illumination architectures (lateral scanning of vertical illuminating light as in above mentioned modalities vs. horizontal illumination in light sheet scanning microscope [7]). As each modality and architecture have their own pros and cons [8–10], several combinations of these methods have been offered at the expense of increased complexity and cost in order to optimize some application-specific considerations such as optical sectioning capability, imaging speed or penetration depth [11–13].

Confocal microscopy (CM) was first introduced in 1957 by Minsky [3, 4], offering a powerful optical sectioning and contrast over wide field microscopy by eliminating the background light using a pinhole. The main advantage of the confocal microscopy over two-photon and OCT is of improved resolution [14] by reducing out of focus light using a pinhole to reject out-of-focus contribution but at the cost of penetration depth (due to lower and high scattering wavelength utilized in CM as opposed to its two-photon and OCT counterparts).

Since the early works on 3D CM, spinning disk confocal microscopy (SDCM) which uses a spinning array of pinholes over the entire field of view has been widely used for video-rate imaging(30fps). However, the SDCM is not as flexible as the laser scanning method due to the limited number of the pixel on the disk and the fixed pinhole size, and the cross-talk between adjacent pinholes decreases the optical sectioning ability [15]. Laser scanning confocal microscopy(LSCM) is based on scanning of the focused laser spot over the object by typically utilizing galvanometer mirrors. Besides, various types of scanning devices such as MEMS-based or piezo-fiber actuators and rotating micro-motors have been developed toward endoscopy or portable microscopy applications, providing fast imaging speed and compactness [16].

While confocal microscopy is a powerful tool in terms of its optical sectioning property up to 1-2 μm, it is not effective for imaging deep into scattering mediums. In addition, the illumination of whole depth while acquiring every single pixel of the image potentially causes photobleaching and phototoxicity problems [17].

An alternative method for deeper imaging is two-photon microscopy which based on the absorbance of two-photon at the focal point simultaneously, therefore rejecting out of focus fluorescence without needing a pinhole. By this nonlinear optical process, one can image deeper tissues up to 1mm as a result of less scattering of near-infrared light. However, the simultaneous two-photon excitation requires expensive high-power, ultra-short pulse lasers [18].

Another method for 3D imaging of biological tissues is optical coherence tomography (OCT) which is based on low coherence interferometry and allows fast volumetric imaging. As the contrast and resolution ($10\mu m$) provided by OCT is not sufficient for cellular imaging and resolution enhancement cannot be accomplished without sacrificing the DOF, the combinations with confocal microscopy and two-photon microscopy have been presented in the literature [12, 13, 19].

1.1 Gaussian and Bessel beams

Gaussian beams are the most common beams employed in a variety of medical imaging methods ranging from wide-field microscopy to super-resolution microscopy. Performing a Fourier transformation to the Gaussian beam does not change its shape and such property enables maintaining the same profile along through a lens system, resulting in a minimal spot size at the focal point and better resolution than other higher-order modes. An ideal Gaussian intensity profile can be denoted by the fundamental transverse mode and the output of a single-mode fiber exhibits a very close approximation to TEM_{00} leading to numerous applications of fiber scanning microscopy. Gaussian beam theory defines two parameters to characterize the beam propagation (Fig. 1.1), beam waist size (w_0) which is the beam width at the focal point ($z = 0$) and Rayleigh range (z_R):

$$w(z) = w_0 \left[1 + \left(\frac{\lambda z}{\pi w_0^2} \right)^2 \right]^{\frac{1}{2}} \tag{1.1}$$

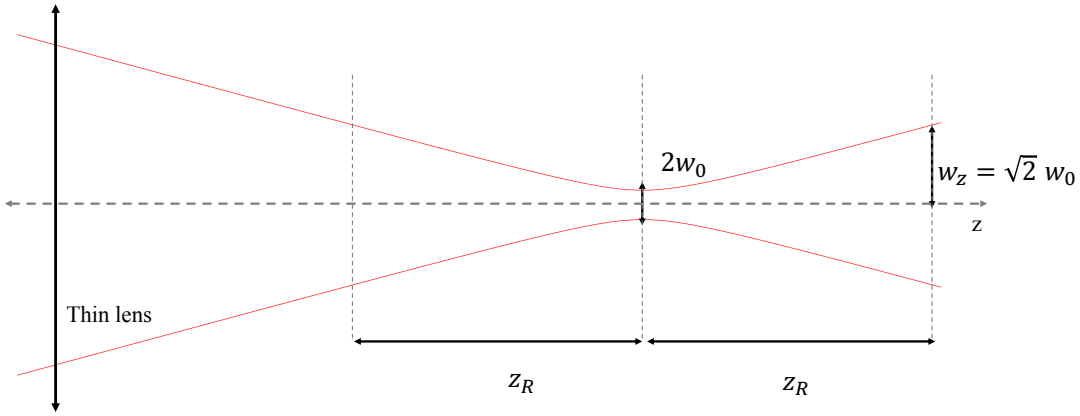

Figure 1.1 : Gaussian beam propagation.

$$z_R = \frac{\pi w_0^2}{\lambda} \tag{1.2}$$

where z is the axial distance from the focus, λ is the wavelength of light, w_0 is the waist radius, and $w(z)$ corresponds to the radius of the beam at z, where the amplitude decreases by $\frac{1}{e}$ with respect to axial value. The Rayleigh range z_R denotes the propagation distance of the beam where its cross-sectional area doubles itself.

Although the Gaussian beam profile has been used in many imaging methods including confocal microscopy applications because of its advantage of tight focusing, the depth-of-field is not sufficient for fast volumetric imaging. Durnin *et al.* showed, both experimentally and theoretically [20, 21], that Helmholtz equations have a diffraction-free solution class (Eq. 1.3) apart from plane waves. This solution class can be written as:

$$E(r,\theta,z) = exp(ik_z z) J_0(k_r r) \tag{1.3}$$

where J_0 zeroth-order Bessel function of the first kind, r and θ are radial and azimuthal components, z is the propagation coordinate and, k_z and k_r are the longitudinal and radial wavevectors.

In the first experimental demonstration of Bessel beams by Durnin et al, an annular aperture and a lens had been used to utilize the Fourier transform relation between an annular ring and Bessel beam (Fig 1.2). Although this method is straightforward and easy, the more efficient way is to use an axicon lens thus one can benefit the all available energy. Besides these conventional ways, the recent studies in medical

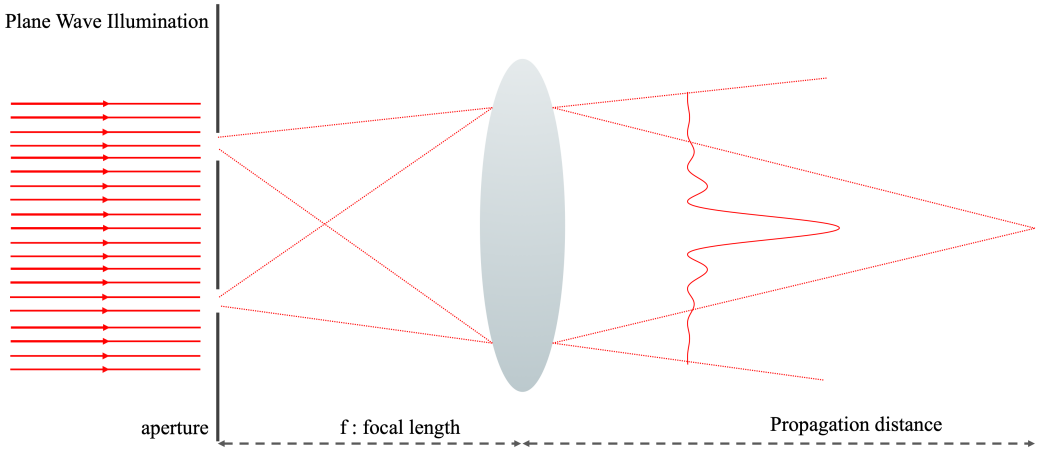

(a)

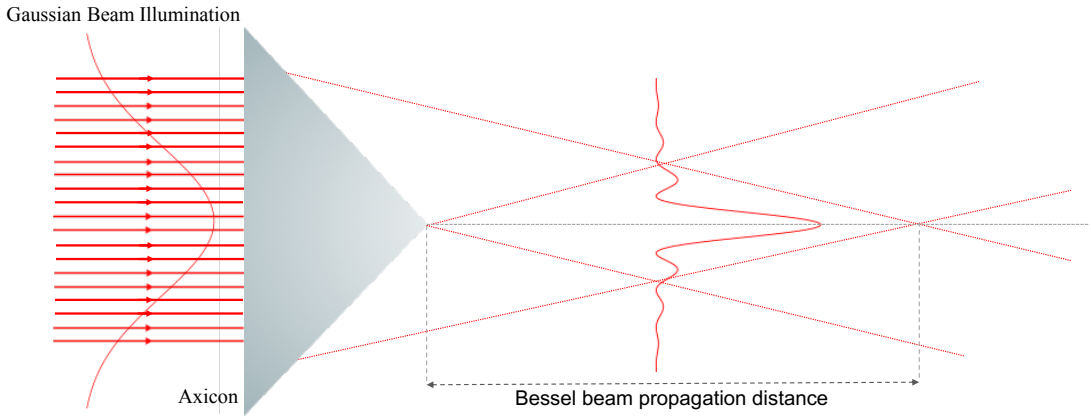

(b)

Figure 1.2 : Generation of a Bessel beam by using a) an annular aperture in the back focal plane of a converging lens and, b) an axicon lens.

imaging have focused on SLM based methods because of its ability of amplitude and phase modulation on incident laser beam [22]. An alternative approach in the formation of Bessel beams for miniaturized systems is to utilize multimode optical fibers in order to avoid additional free-space optical elements. The transmitting light in a multimode fiber comprises multiple spatial modes due to the large core size therefore the output beam suffers from mode dispersion and wave distortion. Nevertheless, by the theory of light propagation in a distorted medium [23], multimode fibers have been widely studied as a beam shaping tool, especially for imaging applications. A number of research groups have employed MMF successfully for the generation of Bessel beams [24, 25].

Ideal Bessel beams carry an infinite number of concentric rings around the propagation axis and thus infinite energy. This energy distribution on the transverse plane

allows the beam to resist the diffraction effect and to reconstruct itself during propagation so-called self healing effect [26]. The improved penetration depth ability for microscopy applications has been demonstrated experimentally in heterogeneous mediums such as human epidermis skin [27] and mouse esophagus tissue [28].

According to Durnin's solution, nondiffracting beams have an extremely narrow central spot, on the order of one wavelength in free space. Experimentally realizable Bessel beams so-called quasi-Bessel or truncated Bessel beams can possess finite energy thus limited propagation distance and thicker central lobe. Gori and Guattari presented an alternative theoretical solution for physical diffraction-free beams, so-called Bessel-Gauss beams [29].

In comparison to Gaussian beam, Bessel beam resists the diffraction effect along far longer distances because of the non-spreading property of the central lobe (Fig. 1.3). However, the unique nature of diffraction free beams brings with it contrast degradation inherently due to the distributed energy among the side lobes. In the recent decade, several methods have been proposed to mitigate this effect and enhance image quality.

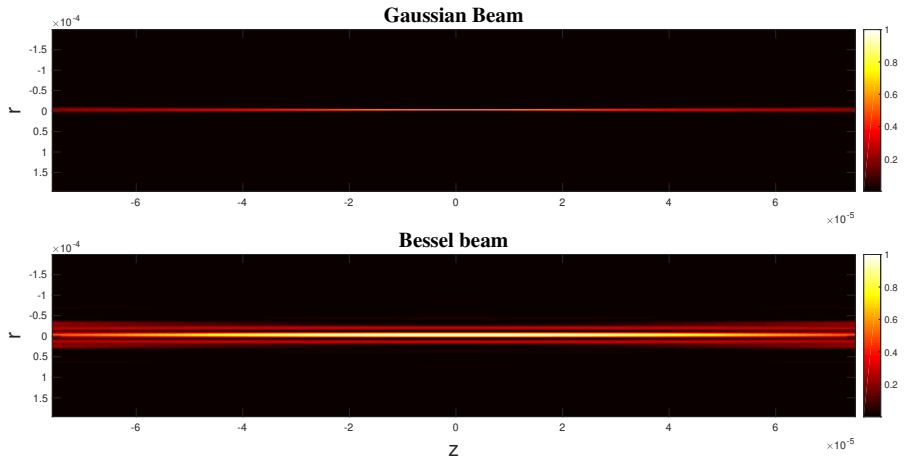

Figure 1.3 : Propagation of a Gaussian (focused using a lens of NA=0.2) and a Bessel beam (generated by Fourier transform of an annular aperture with $\varepsilon = 0.9$) along z. [2]

1.2 Literature Review

The diffraction nature of light is the common obstacle behind deeper images and long FOV therefore Bessel beams have become highly popular with its diffraction-free and self-healing feature among developmental researchers. By incorporation of an axicon lens system into a conventional confocal microscopy system, the resolution has been increased by 20% (0.39λ) compared to Gaussian-based confocal microscopy [30]. A similar axicon-based approach to replace the Gaussian beam with Bessel beam has been proposed for two-photon microscopy and OCT to elongate the focus depth (8 μm res along 4mm DOF [31]) or to increase the lateral resolution while maintaining the depth of field(DOF). ($1.5\mu m$ res over $200\mu m$ DOF [32]). In light-sheet microscopy, Bessel beams have been used extensively in order to achieve homogeneous thin light-sheets thus allowing deeper penetration into scattering objects [33, 34]. The image contrast analysis of Bessel and Gaussian beams for OCT have been reported for equal input power and the same resolution at the focus [35]. Due to the side lobes of the Bessel beam, the background light degrades the contrast in a turbid media more than that of the Gaussian beam. Consequently, the major challenge in using Bessel beams is the rejection of out-of-focus light which originates from the ring-shaped cross-sectional beam profile.

To overcome this shortcoming, a variety of methods have been offered ranging from beam shaping to combinations of different imaging modalities. Recently, annular beam behavior for different beam ratios (defined as the proportion of inner radius to the outer radius) has been investigated to reduce the signal to background ratio(SBR) in multiphoton microscopy. This study uses a spatial light modulator to control the beam ratio ranging from 0 to 1 in which the beam profile can be shifted from Gaussian to Bessel. For extended focal depth and minimum SBR without sacrificing resolution, the beam ratio should be chosen below 0.6 [36] . A similar approach with droplet beams generated by two annular apertures has been presented to suppress background illumination in light-sheet microscopy. The interference of the created co-axial Bessel beams enables the two-fold better contrast by canceling the side lobes [37, 38]. Alternatively, different beam forms such as Sectioned Bessel beams (SBB) or a dual

scanning technique with complementary Bessel beams have been offered to enhance contrast [39, 40].

The incorporation of SPIM (selective plane illumination microscopy) with confocal technique, so-called confocal line detection, has been presented in a number of studies by using a physical slit, a gaussian mask, or using a CMOS camera in the rolling shutter mode [41–43]. These methods obtain the whole image by recording each line separately and, require post-processing, therefore degrades the imaging speed. In another approach, scanned Bessel beams in a SPIM-TPM system have been employed, demonstrating $0.3\mu m$ isotropic resolution in living cells, which comes at the expense of greater complexity and cost [44].

1.3 Motivation

Offering significantly extended depth-of-focus, Bessel beams have been of interest to the biomedical optics community. Bessel beams, created either by use of passive (i.e. axicons) or active (i.e. spatial light modulators) have been utilized in both light-sheet microscopy [45] and laser scanning (confocal or multi-photon) scanning microscopy [46]. Though lateral scanning employing a Bessel-beam is disadvantageous in terms of causing elongated focal spots in the axial direction, it indeed provides significant benefits in i) fast imaging of target tissues having sparsely placed content (i.e. neural tissue) [[47] ii) providing improved rejection of out-of-focus background light as opposed to a Gaussian beam [48], iii) offering improved robustness against deflection at light obstructing objects within the target, mitigating shadowing effects [49], iv) capability of producing higher speed stimulated emission depletion imaging for super-resolution imaging [49].

First, a robust optical architecture has been demonstrated to map the laser beam to multiple Bessel-like beams at different depths for improved imaging speed. The heart of the proposed method lies in producing a higher order Bessel beam comprising concentric light rings via off-axis coupling light into a multi-mode fiber (MMF). The higher-order Bessel-Beam is then focused onto the target via a spherical lens, which maps each ring to different depths owing to its inherent aberration. Thus lateral scan of the fiber results in multiple depths of the target to be scanned at once and this improves the imaging speed in comparison to a conventional confocal microscopy system.

Secondly, a mode-optimized two-dimensional piezoelectric fiber actuator and a novel actuation scheme have been studied in order to establish three different scan patterns (Lissajous, spiral, and raster) with the same device. The flexibility in choosing scan patterns offers multiple options for the operator to choose between improved uniformity, high frame-rate to image abrupt biological applications, or circular field-of-view to better image naturally cylindrical cavities (gastrointestinal tract, esophagus, etc.). The presented device, along with the actuation strategy is a promising candidate for integration with miniaturized laser scanning devices towards clinical use.

Overall, the combination of these two architectures enables a miniaturized, multi-pattern 3D imaging system as a result of the compactness of the piezo-fiber scanner system and the lack of extra free optical elements in forming Bessel beams.

2. SYNCHRONOUS IMAGING OF MULTIPLE SLICES WITH SINGLE LATERAL SCAN USING HIGHER-ORDER BESSEL BEAMS AND A SPHERICAL LENS

2.1 Proposed Architecture

The heart of the proposed architecture lies in simultaneous use of a multi-mode fiber and a spherical lens, as illustrated in Fig. 2.1. Multi-mode fiber allows for generation of higher-order Bessel beams. Various techniques have been employed in literature to create higher-order Bessel beams via MMF's, through first coupling light into a single mode fiber spliced onto a MMF [24], or employing coupling the interference pattern between dual pig-tailed fibers into a multi-mode fiber [50]. Here, we coupled light in an off-axis fashion, resulting in a higher-order Bessel-like beam, whose number of concentric rings, as well as ring spacing is controlled via tilt, and translation stages.

The spherical lens maps each light ring to different depths, allowing for creating multiple foci from single input beam. Thus altering the distance between rings through varying coupling conditions, the distance between the foci's of the spherical lens also changes.

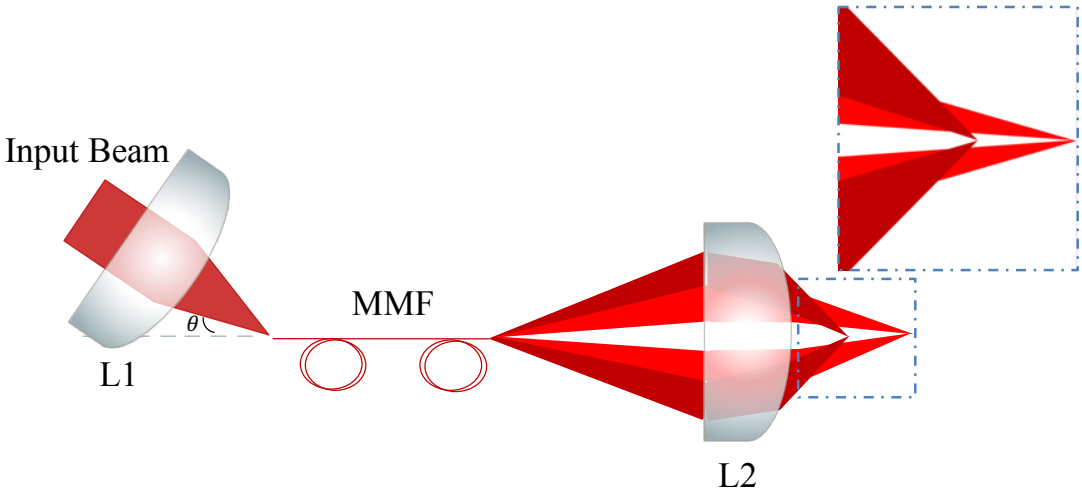

Figure 2.1 : The proposed architecture: off-axis coupling for generation of higher-order Bessel-like beam and a spherical lens to map each optical ring to a distinct focus.

In the next section, we'll introduce how the architecture is utilized for a scanned optical imaging scenario, in demonstrating acquisition of data from multiple depths with a single scan.

2.2 Experimental Setup

The setup, illustrated in Fig. 2.2., builds upon the proposed architecture. Lower numerical aperture (NA) portion of the coupled light is mapped to the inner optical ring observed at the output of the MMF, while the peripheral portion of the incoming light is mapped to the outer optical ring. The distal end of the MMF is attached to a piezoelectric cantilever [51] for scanning the higher order Bessel spatially along the final focusing spherical lens. Note that the output of the fiber is first collimated via an objective lens (20x, NA = 0.4) and then focused using the spherical lens (f = 50 mm). Without loss of generality, the collimation and focusing optics could be replaced to achieve desired lateral and axial resolution at the target. As the target we've utilized either i) a mirror that is translated along the optical axis or ii) multiple resolution targets each placed at a distinct focus. The reflected light re-couples into the fiber. Finally, The beam splitter that is placed right after the laser light source enables directing the reflected light towards two photo detectors, each of which capture light coming from different focus with the help of beam blocs (spatial filters) eliminating light arriving from the other focus. The photo detectors are connected to a two-channel oscilloscope to monitor data acquired from different depths, simultaneously. Additionally, a CMOS

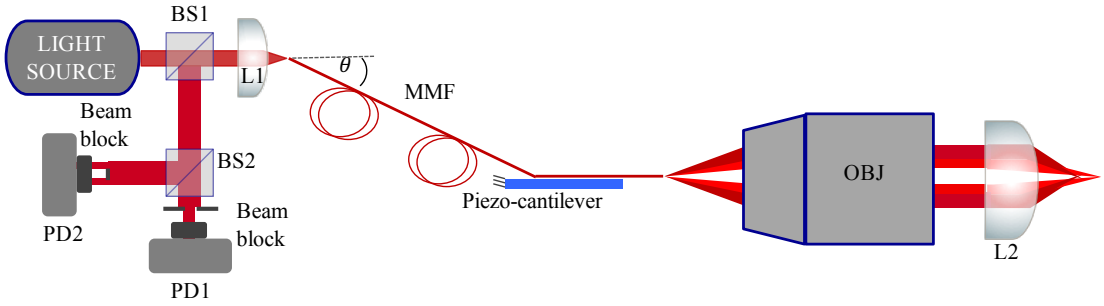

Figure 2.2 : The experimental setup, utilizing a piezoelectric based fiber scanning mechanism to spatially scan light on the target, two photodetectors each of which is mapped to a different focus, and the target (a mirror, or a resolution target); BS: beam splitter, PD: photodetector, OBJ (objective lens), and bem blocks refer to spatial filters that eliminate light arriving from the other focus.

camera is placed beneath the target to monitor the position and size of the scanned beam on the target.

2.3 Results

Using a mirror that is placed on a translation stage along the optical axis as the target we've first recorded the light intensity using both photo detectors. Each photodetector signal exhibits a maximum corresponding to the location where the mirror coincides with one of the foci. We repeated the procedure for a number of different MMF outputs (through altering fiber coupling conditions, i.e. altering the translation and tilt knobs) showcasing two nested rings, spaced at different radial position. Fig. 2.3 illustrates the acquired signals (for various MMF outputs) from both foci as the mirror translates. As expected, optical rings that are closely separated create two foci that are adjacent, whereas further apart separated rings result in distant foci. In the next

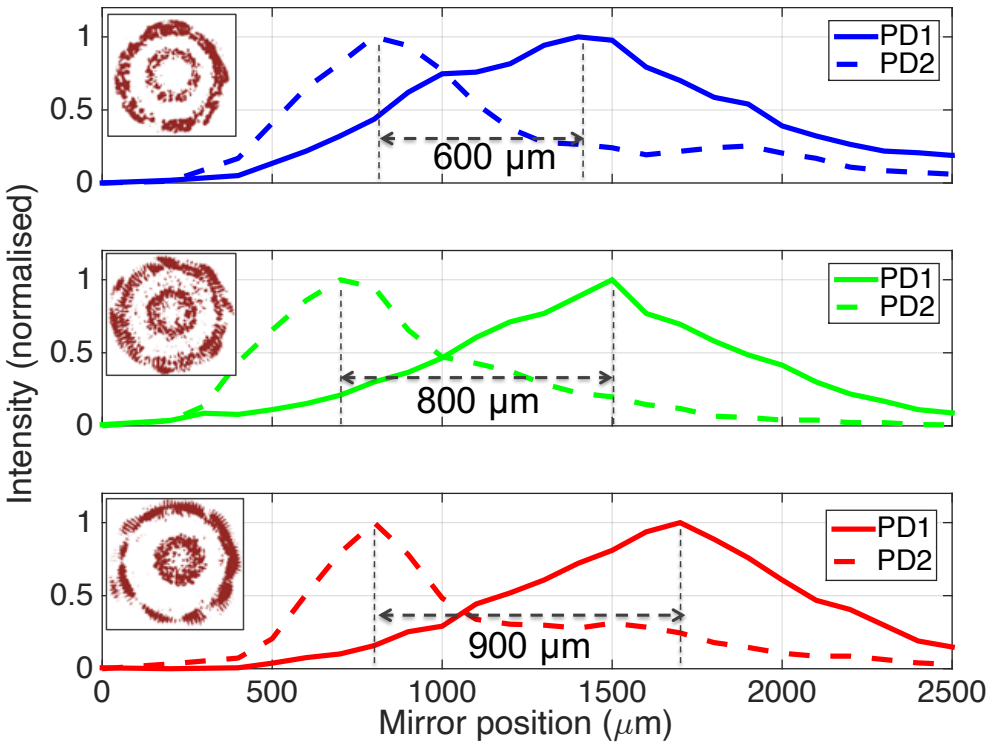

Figure 2.3 : Acquired signals (for various MMF outputs shown in the insets) from both photodetectors as a function of mirror position. Optical rings that are closely separated create two foci that are adjacent, whereas further apart separated rings result in distant foci.

step two back-to-back United States Air Force (USAF) resolution targets were placed, each of them corresponding to a focus. The piezoelectric fiber scanner, having an

extended MMF length of 10 mm was driven at 1.5 kHz frequency. Fig. 2.4 illustrates the placement of the USAF targets, the location of the scanned beam (based on the observation via the CMOS camera), along with the light intensity data acquired by both photodetectors and the oscilloscope. Our findings reveal successful signal acquisition from both channels corresponding to coaxially located stripe patterns on each USAF. As detailed in Fig. 2.4c, the first photodetector (PD1) that is capturing light from the rear focus does not receive any light for the region (labeled as region I) where the target located at the front focus (Target 2) blocks the rear focus (Target 1). On the other hand regions II, III, and IV result in a consecutive increase-decrease-increase in the signal intensity as a result of the stripes showcased by Target 1, for PD1 signal. On the other hand, PD2 that is monitoring the front focus (Target 1), showcases a high intensity signal at region I due to reflective part of Target 1, and lower intensity signal at regions II, III, IV as Target 1 is transparent in those regions and the defocused beam does not pick any alternating signals as in PD1. Note that the reflected peak observed at PD1 from region IV of target 1 possess higher intensity than the reflected peak for region III mainly due to the bandwidth limit of the photodetector. As region IV corresponds to the edge of the scan-line, higher intensity is collected due to slowed-down motion of the fiber.

2.4 Discussions and Conclusion

In this study, a novel optical architecture was showcased utilizing a higher-order Bessel-like beam that is generated with off-axis coupling into an MMF fiber, along with a spherical lens to map each optical ring to distinct foci. Through altering the tilt and the translation of the fiber coupling mechanics, it is possible to change the optical ring spacing, which in turn alters the axial distance between foci's. Moreover, we have successfully demonstrated simultaneous data acquisition from two target planes with a lateral scan.

The beam scanning was accomplished using a piezoelectric cantilever on which MMF was fixed. Though we've performed a 1D light scan, the lateral scanning can easily be adopted for 2D using a piezoelectric tube [52], or orthogonally placed piezoelectric cantilevers [1]. The presented scanning and higher-order Bessel-like beam forming

strategies allow for compact implementation of the proposed architecture, which is appealing particularly for endoscopic applications.

Though the demonstrations were carried out for acquiring simultaneous data at two different planes, without loss of generality the methodology allows for higher number of (> 2) planes to be acquired at a single lateral scan, at the expense of necessitating higher optical power at the input. Moreover, each plane could be acquired based on a different modality, i.e. fluorescence characteristics could be acquired for one plane whereas reflectance data could be sought in another upon using proper filtering options at each photodetector. As a particular example two-photon fluorescence imaging can be used for the epithelial layer to reveal cellular structure near tissue surface meanwhile second-harmonic-generation (SHG) imaging of the extracellular matrix beneath the epithelium to reveal collagen distribution [53], simultaneously.

Note that the coupling conditions also alter the intensity ratios of the optical rings, thus special attention must be given to ensure that the deeper focus receives greater optical power, as it will be scattered and observed more than the shallow focus.

In this study, we've demonstrated proof-of-principle data acquisition to showcase the efficacy of our method, on binary resolution targets. Experimental demonstration of the presented methodology in biological tissues will be performed as a future work.

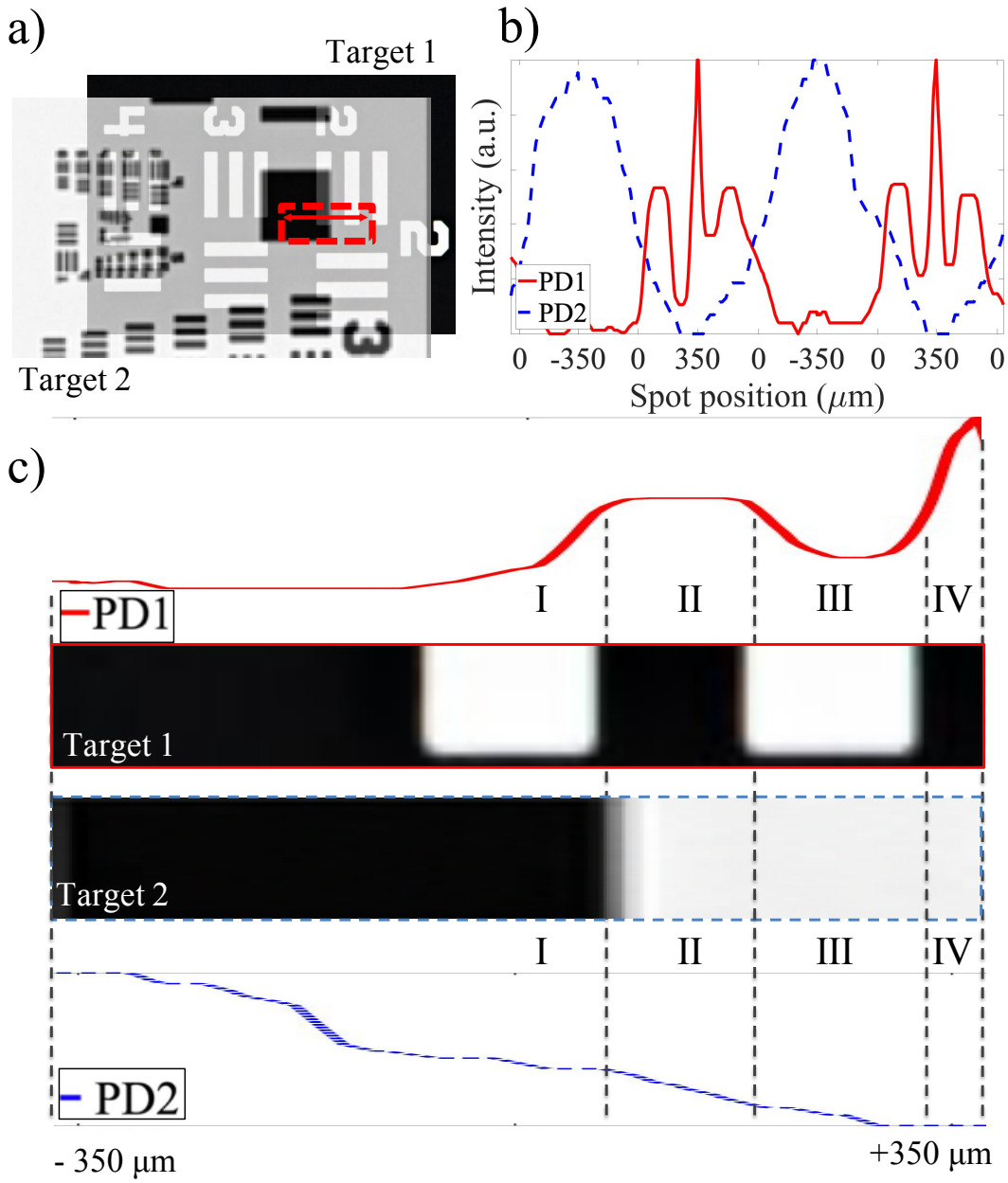

Figure 2.4 : Simultaneous acquisition of cross-sectional reflection data from two USAF targets located at different foci (the location of the scan-line is shown with the arrow): a) alignment of the targets b) acquired signal from both photodetectors c) A close-up view of the scanned line (for half a scan period) and the corresponding photodetector signals. Dashed (left-side) region corresponds to target 2, which is responsible from portion highlighted as "I" of the photodetector signals. The regions II, III, and IV are transparent in target I and reflective-transparent-reflective, respectively, in target II. Note that dark and light regions correspond to reflective and transparent parts of the USAF targets.

3. MULTIPLE-PATTERN GENERATING PIEZOELECTRIC FIBER SCANNER TOWARDS ENDOSCOPIC APPLICATIONS

Spiral scanning pattern has been mostly preferred over raster scanning in piezoelectric cylinder actuator based fiber scanning endoscopes. The cylindrical geometry of the fiber optical cable results in identical mechanical resonances in orthogonal directions, leading to a circular scan pattern when 90 phase difference is applied between orthogonal electrodes. Once the drive signal amplitude is altered the diameter of the circular patterns shrink / enlarge, forming a spiral scan pattern [54]. Lissajous scanning is yet another alternative to raster and spiral scanning, where both orthogonal axes are scanned in a resonant fashion [55].

Figure 3.1 illustrates raster, spiral, and Lissajous patterns along with their main advantages and dis-advantages. In summary, a raster scan provides uniform illumination, while necessitating high drive voltage and a broad-band ramp signal for the actuation of the slow axes that is prone to detrimental measurement noise [56]. With its circular FOV, spiral scan provides a great match-up in imaging cylindrical body cavities, dedicating the entire FOV. In contrary, with a rectangular FOV, nearly one quarter of the FOV remains empty, while imaging a cylindrical body cavity. On the oth-er hand, spiral scanning shows poor performance in image uniformity,

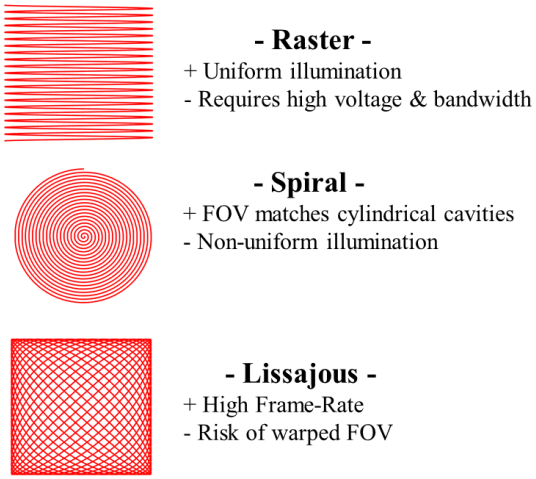

Figure 3.1 : Visualization and comparison of different scan patterns [1].

possibly requiring tailoring of the laser intensity at different instants of the scan. Finally, Lissajous scanning is capable of sub-frame rate imaging for enhanced dynamic information and reduced blur, at the expense of reduced fill rate, i.e. partial filling of the FOV [55] . Also, as the vertical and horizontal mechanical resonances of a fiber are near identical, Lissajous scanning of a fiber is prone to coupling between orthogonal modes, resulting in a warped Lissajous pattern. While the scientific literature regarding LSE research have focused on a single scan pattern per presented device, it is a crucial asset for the endoscopic device to be able to switch from one scan pattern to another de-pending on whether uniformity, high frame-rate or having a circular FOV is critical.

3.1 The Piezoelectric Fiber Actuator

3.1.1 Geometry

Figure 3.2 illustrates the actuator that is used throughout this study; comprising two orthogonally placed piezoelectric bimorph cantilevers, and an extended fiber cable. Note that an actuator with a similar geometry had been utilized in multi-photon endoscopy [57], however, limited to performing raster scanning only at about 4 frames-per-seconds (fps). Our choice of cantilever and extended fiber dimensions (presented in Table 3.1), along with the presented mode optimization and actuation strategy allows for i) 256 x 256 pixel scan at 20 fps for raster scanning, ii) 256 pixel diameter spiral scan at 20 fps, and iii) 256 x 256 pixel scan at 50 fps with 50% fill rate. Furthermore the presented actuator is mode-optimized to ensure immunity to environmental noise and improved electro-mechanical conversion efficiency.

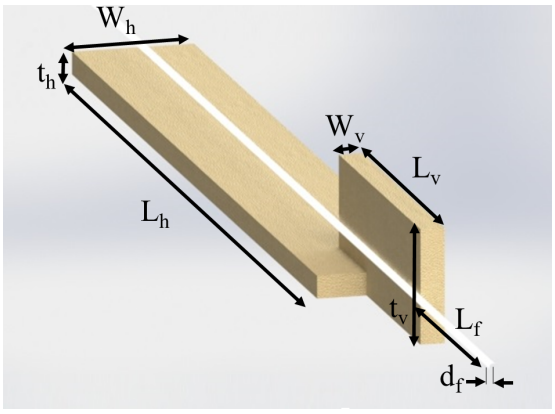

Figure 3.2 : The piezoelectric fiber actuator [1]

Table 3.1 : Geometrical and material property values for the piezoelectric actuator [1]

Parameter	Description	Value
L_h	Length of the horizontal cantilever	20 *mm*
W_h	Width of horizontal cantilever	5 *mm*
t_h	Thickness of horizontal cantilever	0.25 *mm*
L_v	Length of vertical cantilever	4 *mm*
W_v	Width of vertical cantilever	5 *mm*
t_v	Thickness of vertical cantilever	0.25 *mm*
L_f	Length of extended fiber	6.1 *mm*
d_f	Diameter of the fiber	125 μm
E_{piezo}	Young's modulus of piezo	49.5 *GPa*
E_{silica}	Young's modulus of silica	73 *GPa*
ρ_{piezo}	Density of piezo	7455 kg/m^3
ρ_{silica}	Density modulus of silica	2200 kg/m^3

The cantilever lengths were chosen to enable actuation of the fiber at reasonable voltages (< 50 Vrms, see next section for details of mode optimization). The total rigid length of the actuator is 30 mm, which is comparable to other endoscopic actuators presented in literature [8–10]. Note that our actuator potentially could be further shortened down with the use of thinner cantilevers or with piezoelectric materials having higher piezoelectric coefficient.

3.1.2 Modal analysis and mode optimization

Figure 3.3 illustrates the four mechanical modes of the actuator utilized in the scanning operation, simulated with COMSOL software. The modes correspond to the fundamental and the 3rd resonance of the horizontal cantilever, and the fundamental resonance of the extended fiber cable in x and y dimensions. Although a fiber is cylindrical, the non-uniformity in meshing operation results in slightly different mechanical frequencies in vertical and horizontal axes in the simulation results. Practically, the imperfections of the epoxy flow for the stabilization of the fiber onto the cantilever also leads to a difference between horizontal and vertical mechanical frequencies of the fiber. We've previously exploited the use of polarization maintaining fiber that is geometrically circularly asymmetric to further break apart the horizontal and vertical resonances, allowing an unwarped Lissajous scan pattern [58]. However to achieve multiple scan patterns (such as spiral scan pattern that requires excitation

of orthogonal axes with the same frequency), here we sticked with a conventional single-mode fiber.

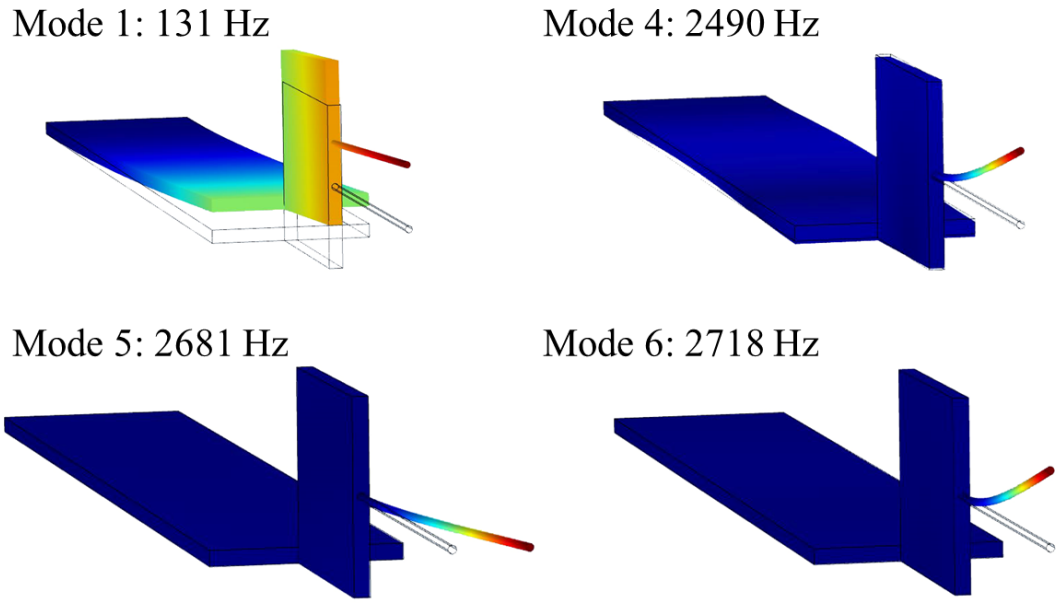

Figure 3.3 : Vibration frequencies of the utilized modes in scanning multiple patterns, corresponding to fundamental and 3^{rd} resonances of the horizontal cantilever, and fundamental fiber modes in horizontal and vertical directions. Intermediate modes that are not utilized are only reported in results section [1].

We exploited a mode-optimization strategy for improved electromechanical conversion efficiency, potentially improving patient safety for a miniaturized invasive device exploiting our actuator, and mitigating voltage requirements for actuation. The following steps highlight the requirements imposed by the actuator and our solution to address these requirements:

1) Achieving reasonable deflection at off-resonance for the slow axis of the raster pattern: Horizontal cantilever length was chosen to provide a fundamental resonance above 100 Hz, offering off-resonance operation in response to a triangular wave at the desired frame-rate of 20 Hz, and ensuring immunity to environmental noise that is typically below 100 Hz [59].

2) Ensuring high electromechanical conversion efficiency for spiral, Lissajous and fast axis of the raster scan pattern: Once again the horizontal cantilever geometry should be tailored to ensure that a higher order mode of the horizontal cantilever is co-located (or located close) to the extended fiber resonance. We've previously showcased through analytical modeling, simulations and experimental results that nearly matching

fundamental or higher-order resonances of the piezoactuator, and the extended fiber ensures improved electromechanical conversion efficiency [51].

In accordance with above two arguments, we've set the cantilever dimensions to the values depicted in Table 3.1, offering a 131 Hz fundamental resonance of the horizontal cantilever and a third order mode of around 2500 Hz that is very close to the fundamental resonance frequency of the fiber, which is about 2700 Hz. Moreover, the horizontal cantilevers third mode offers an extra degree of freedom in frequency selection to accomplish a Lissajous scan. Note that optimization of the Lissajous scan frequencies plays a vital role in ensuring high frame-rate and high fill-factor [60].

3.1.3 Actuation scheme

Figure 4 and Table 2 illustrate the voltage patterns and the applied frequencies to the cantilevers in order to achieve all three scan patterns. A resonant/non-resonant raster scan pattern can be achieved through applying a low frequency triangular wave to the horizontal cantilever while exciting the vertical cantilever at the fiber resonance (f_{fiber}). A spiral scan pattern is achieved through driving both cantilevers at or near the fiber resonance (f_{fiber}), with a 90 phase shift and applying a triangular (or sinusoidal) amplitude modulation to achieve set of concentric circles. Finally, the Lissajous pattern is produced through applying slightly off-resonant frequencies (f_{fiber+} and f_{fiber-} , two frequencies that are slightly higher and lower than the fiber mechanical reso-nance). One can tailor f_{fiber+} and f_{fiber-} to achieve different Lissajous patterns in order to optimize fill factor of the scan as well as the coupling between horizontal and vertical axes. The adjustment of drive frequencies in a Lissajous scan for both axes would alter the FOV, which could be compensated with altering the drive voltage. The presence of the extra resonance peak due to the 3rd mode of the horizontal provides a broadened set of frequencies from which a wider range of Lissajous scan frequencies could be selected to achieve desired frame vs. fill-rate metrics.

Raster scanning endoscopes have exploited non-resonant / non-resonant raster with excellent uniformity, at the expense of a very low frame rate (0.1 fps) [61]. This study exploits a resonant / non-resonant scanning to generate a raster pattern, for improved speed, with some compromise from uniformity. On the other hand spiral and Lissajous patterns are implemented in the conventional manner.

Table 3.2 : Waveforms and frequencies applied to the actuator for different scan patterns

Parameter	Raster	Spiral	Lissajous
Vertical waveform	$tri(2.fps.t)^*$	$sin(2\pi f_{fiber}t).tri(2.fps.t)$	$sin(2\pi f_{fiber+})$
Horizontal waveform	$sin(2\pi.f_{fiber}t)$	$cos(2\pi f_{fiber}t).tri(2.fps.t)$	$sin(2f_{fiber-})$

** triangle function (with 1 second period). Alternatively a sinusoidal function could be utilized to ensure smooth from downward to upward motion.*

*** Alternatively 3_{rd} mode of the horizontal cantilever: f_{mode4} could be (and has been in the experimental results) utilized for extra benefits as described in the manuscript.*

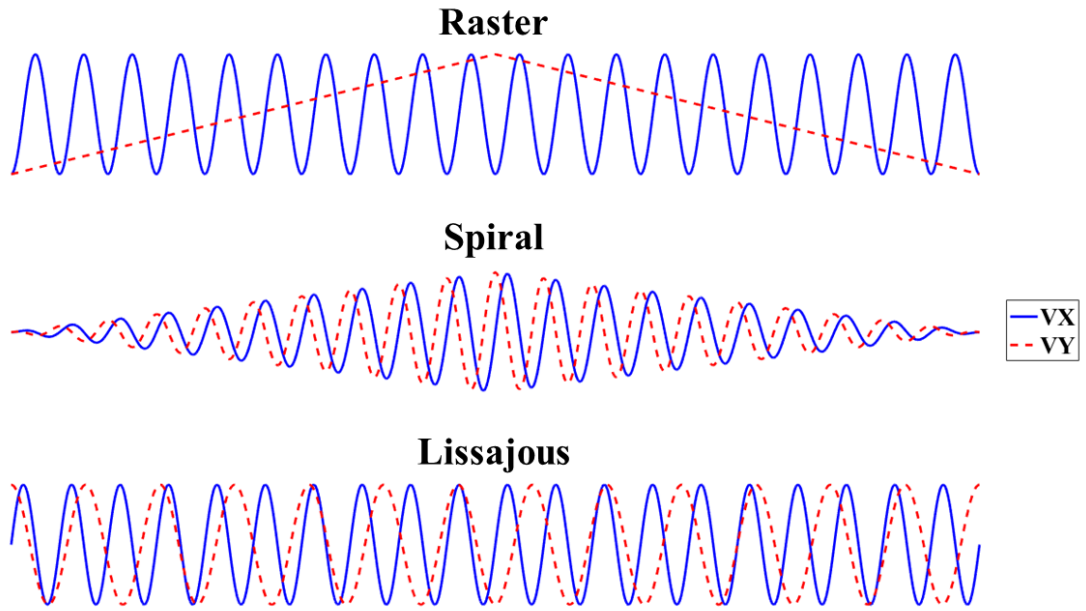

Figure 3.4 : Actuation scheme for all scan patterns, showcasing voltages applied for vertical (V_x) and horizontal (V_y) excitation [1].

3.1.4 Image metrics with different scan patterns

The number of resolvable spots (in one dimension: N) of a resonant / non-resonant raster pattern (N_{raster}), exploiting the actuation waveforms, summarized in Table 3.2, can be calculated as:

$$N_{raster} = \frac{f_{fiber}}{f_{fps}} \tag{3.1}$$

Thus to achieve a raster scan with 20 fps, one should apply a 10 Hz triangular wave to the horizontal cantilever (which indeed moves in the vertical direction). Both up-slope and down-slope parts of the triangle function correspond to different frames, such that raster pattern is scanned in different slow-scan directions for the consecutive frames. Alternatively, a ramp function can be applied as opposed to the triangle to ensure that

all frames are collected identically. Yet, ramp function requires an abrupt decline near the end of the period to return to its original po-sition that would require an even increased bandwidth (and thus detrimental noise) actuation signal. To achieve $N_{raster}^2 =$ 256x256 resolvable spots at 20 fps, the fiber should be actuated in the hori-zontal direction at 2560 Hz. The fundamental mechanical resonance of the extended fiber can be calculated through [57]:

$$f_{fiber} = \frac{3.52 d_f}{8\pi {L_f}^2} \sqrt{\frac{E_{silica}}{\rho_{silica}}} \tag{3.2}$$

Thus, based on Eq. 3.1 and the silica fiber material properties depicted in Table 1, the fundamental the extended fiber length is chosen as 6.1 mm. The number of resolvable spots of a spiral pattern (N_{spiral}), can be calculated in a similar manner to the raster case based on Eq. 3.2, as evident from Fig. 3.4. The frame-rates of raster and spiral patterns are directly based on the slow-scan or amplitude modulation of the actuation signals, whereas that of the Lissajous pattern depends on the largest common divisor of the actuation frequencies in orthogonal directions. Yet, it is possible to benefit from sub-frame-rate Lissajous imaging 6 to better acquire dynamic information at the expense of reduced fill rate (amount of pixel scanned by the laser versus total pixels in the FOV). Previous arguments have shown that one needs a fiber resonance of 2560 Hz, corresponding to 6.1 mm extended fiber length, to achieve $N_{raster} = N_{spiral} = N_{lissajous} = 256$, at 20 fps for raster and spiral patterns and potentially higher fps for the Lissajous scan (see results for a discussion on the frame rate of the Lissajous scan). One other criteria to satisfy the given resolvable spot size is as follows:

$$FOV = N.\delta_{xy} \tag{3.3}$$

where δ_{xy} is the full-width half maximum (FWHM) focused laser spot on the target. The results section will detail how the acquired data compares to the results theoretically obtained from Eq. 3.1-3.3.

3.2 Experimental Setup

To demonstrate the multi-pattern scan capability of our actuator we built the setup that is illustrated in Fig. 3.5. A laser diode (1mW power, 630 nm wavelength) is coupled

into a single-mode fiber (Thorlabs SM600) via an objective lens (NA = 0.17). The distal end of the fiber was attached at the tip of the actuator with subtle amount of epoxy. The tip of the distal fiber was first mapped onto a United States Air Force (USAF) resolution target and then to a CMOS camera using two convex lenses. The first lens (f = 35 mm) images the fiber tip, having 2 μm FWHM mode-field diameter (according to fiber specs) with 1:10 magnification, to achieve a 20 m spot at the conju-gate plane, where USAF target is located. The actuation voltage was measured as < 50 V_{rms} voltage at the piezo cantilevers for all scan patterns to achieve a FOV of 5.12 mm, which corresponds to N=256, based on Eq. 3.3. As the CMOS camera pixel size is 5 μm, each laser spot is thus sampled with 4x4 pixels, and the FOV is sampled with 512 x 512 camera pixels. The second lens maps the USAF target onto the CMOS camera with unity magnification. The role of the resolution target and the CMOS camera in the setup is to visualize the uniformity and frame-rate of different scan patterns.

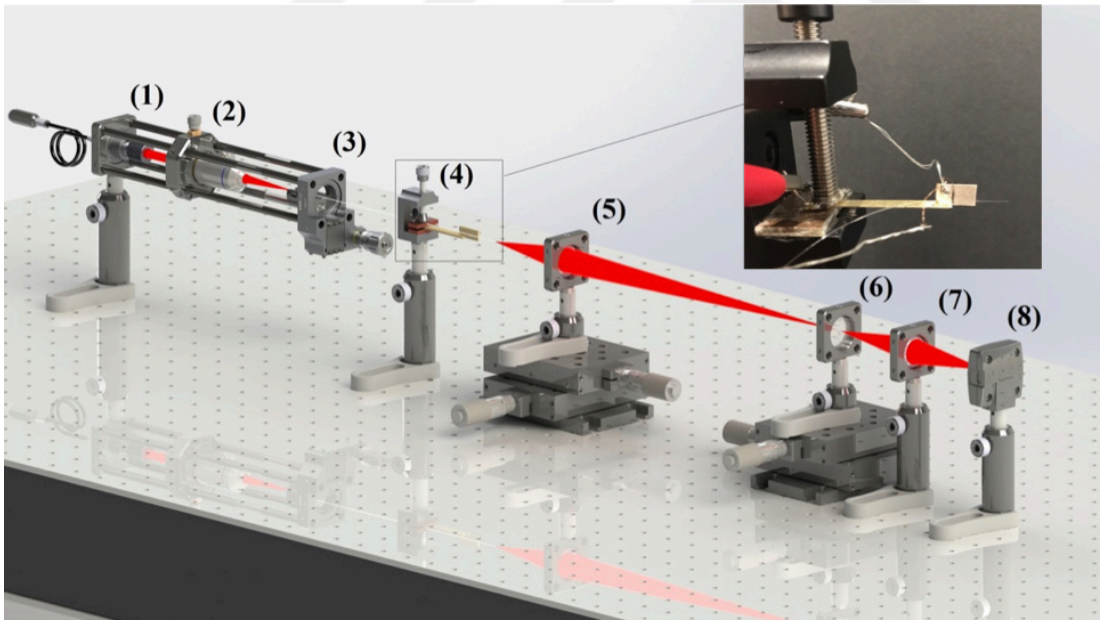

Figure 3.5 : Experimental setup comprising: (1) laser diode, (2) objective lens, (3) single-mode fiber, (4) 2D piezoelectric fiber actuator (magnified in the inset), (5) lens 1 (f = 35 mm), (6) USAF target, (7) lens 2, (8) CMOS camera [1]

3.3 Results

This section summarizes the characterization results of the presented actuator and the proposed actuation for multi-pattern scanning.

3.3.1 Mechanical frequency response of the actuator

The frequency response in vertical and horizontal directions was acquired through sweeping the actuation frequency in orthogonal directions, and recording the length of the scan-line. As presented in Figure 3.6, the acquired frequencies are close to those achieved with FEM results. We attribute the slight difference between the simulated and experimented values for the horizontal fiber resonance to the effect of boundary condition at the cantilever end of the fiber due to the spreading of the epoxy (effectively altering the extended fiber length). As previously discussed, the horizontal cantilever length was deliberately chosen to make sure that last two modes (up till 3000 Hz) observed in vertical directions is nearly co-located, offering an improved electromechanical conversion efficiency and larger set of frequency options for the Lissajous scan. On the other hand only a single mode is observed in the horizontal direction. Extra parasitic modes (observed in the experiments only) at 2300 and 2700 Hz exhibiting rather small displacements were observed for the horizontal scan that may be attributed to a combination of measurement noise and the effects of the loading that the cable wiring presents on the cantilevers. Note that loading from the wiring could be mitigated through the use of wire bonding, to utilize very thin and lightweight electrical connections.

3.3.2 Image uniformity and fill factor with different scan patterns

Once the device is characterized, the actuator is now ready to demonstrate multiple scan patterns. Utilizing the actuation scheme, the presented setup, and the FOV (About 500 x 500 μm^2 at the fiber tip and 5 x 5 mm^2 at the conjugate plane and the CMOS camera) to achieve N2 = 256 x 256 re-solvable spots. Figure 3.7 illustrates all three-scan patterns that are projected onto the USAF target. The raster pattern was actuated with $f_{vertical}$ = 10 Hz (sinusoidal wave as opposed to a triangular wave to

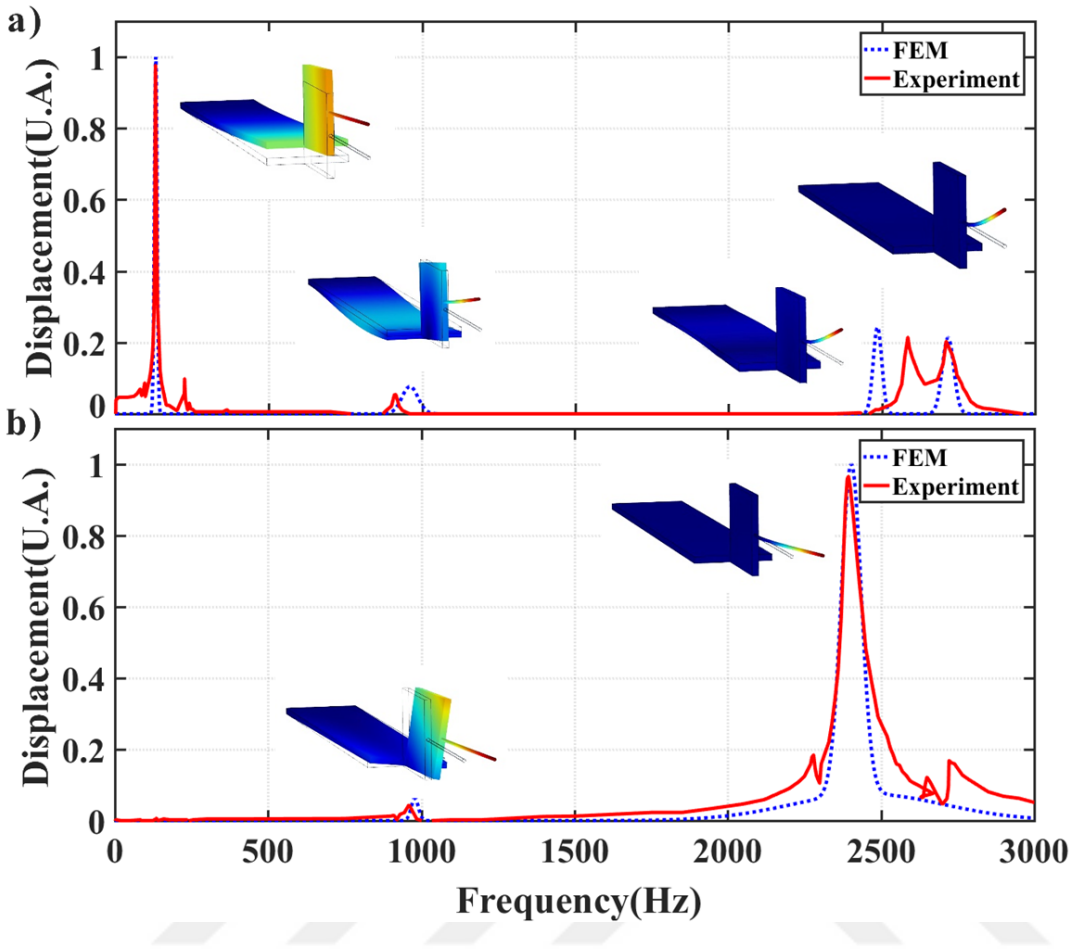

Figure 3.6 : Frequency response of the actuator in a) vertical and b) horizontal directions. Mode shapes and arrows refer to FEM results for comparison with experimentally acquired frequencies [1].

ensure a continuous derivative leading to a smoother transition for the slow-scan) and f_{fiber} = 2667 Hz (sinusoidal), the spiral pattern with f = 2620 Hz (an intermediate frequency between horizontal fiber resonance and the 3^{rd} mode of the horizontal cantilever) for both channels with 90 phase difference and a 10 Hz sinusoidal amplitude modulation for both channels. Finally the Lissajous pattern was actuated with f_{mode4} = 2610 Hz and f_{fiber-} = 2439 Hz, respectively in orthogonal directions. Note that the raster pattern is generated via simultaneous drive of fundamental mode of the horizontal cantilever together with vertical resonance of the fiber. On the other hand there are several options to create spiral and Lissajous scan patterns; where the horizontal fiber resonance could be simultaneously driven with either vertical fiber resonance or the 3^{rd} mode of the horizontal cantilever. Also the drive frequencies used in the experiments slightly deviates from those reported in the mechanical frequency

response section, frequency behavior tends to slightly change for each direction, while the other orthogonal direction is also driven simultaneously.

All frames were captured with 20 fps and 50 msec exposure time of the CMOS camera, while several different fps and exposure time options were attempted with the Lissajous (only 20 fps shown in Fig. 3.7 c). Figure 3.7d. also illustrates frame rate and fill rate analysis [55], for the presented resolution, We refer the reader to another other study for frequency selection rule for enhanced frame-rate [62]. The Lissajous scan provided a 20 fps with near unity fill rate (93%), 30 fps with 70% fill-rate and, 50 fps with 50% fill-rate, and > 100 fps with 25% fill rate, for the selected frequencies and N_2 = 256 x 256. Although 25% fill rate lacks three quarters of the FOV, smart interpolation algorithms have been implemented with Lissajous scan [63], which would have not been possible with any other scan pattern.

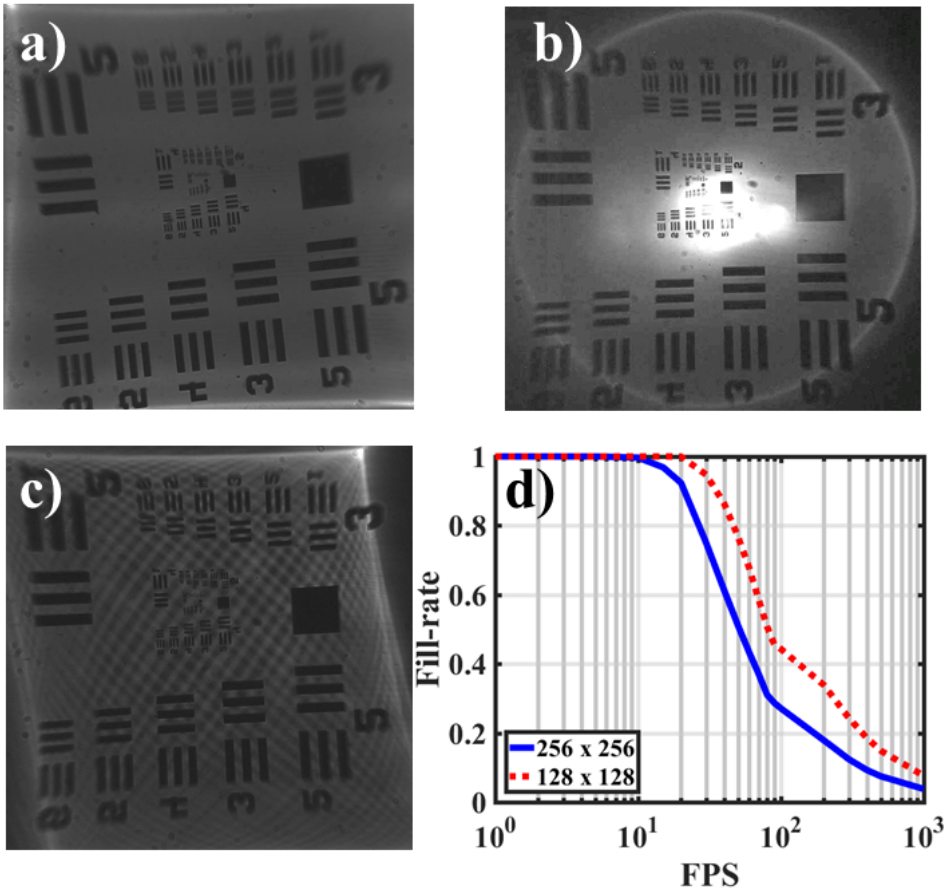

Figure 3.7 : Achieved scan patterns on the target at 20 fps: a) raster scan, b) spiral scan, c) Lissajous scan. Finally d) illustrates fill-rate vs. fps plot for the utilized frequencies in Lissajous scan, for N_2 = 256 x 256, and 128 x 128 [1].

4. CONCLUSION

First, we achieved the generation and focusing higher-order bessel beams at different depths and imaging of multiple planes with single lateral scan using a 1D piezo-fiber scanner. Next, we demonstrated a robust actuation scheme on a mode-optimized (immune to environmental noise and providing good electromechanical efficiency), orthogonally placed, double piezoelectric cantilever based 2D fiber actuator which could be utilized in the first architecture to create a 3D system. We've showcased all raster, spiral, and Lissajous patterns with the device. Such an actuator could be embedded in a laser scanning endoscope to reveal pathological information. With multiple scan pattern options, the device is capable to provide either images with better uniformity, high frame rate (at the expense of fill-rate, to capture dynamic information), or a circular FOV while imaging cylindrical body cavities for effective dedication of the available pixels. Thus, with further development the presented actuator and drive scheme could serve as a useful tool as a part of a minimally invasive opto-medical device in the clinic.

REFERENCES

[1] **Tekpınar, M.**, **Khayatzadeh, R. and Ferhanoğlu, O.** (2019). Multiple-pattern generating piezoelectric fiber scanner toward endoscopic applications, *Optical Engineering*, *58*(2), 023101.

[2] **Sheppard, C.** (1977). THE USE OF LENSES WITH ANNULAR APERTURE IN SCANNING OPTICAL MICROSCOPY.

[3] **Marvin, M.**, (1961), Microscopy apparatus, uS Patent 3,013,467.

[4] **Minsky, M.** (1988). Memoir on inventing the confocal scanning microscope, *Scanning*, *10*(4), 128–138.

[5] **Huang, D.**, **Swanson, E.A.**, **Lin, C.P.**, **Schuman, J.S.**, **Stinson, W.G.**, **Chang, W.**, **Hee, M.R.**, **Flotte, T.**, **Gregory, K.**, **Puliafito, C.A.** *et al.* (1991). Optical coherence tomography, *science*, *254*(5035), 1178–1181.

[6] **Denk, W.**, **Strickler, J.H. and Webb, W.W.** (1990). Two-photon laser scanning fluorescence microscopy, *Science*, *248*(4951), 73–76.

[7] **Siedentopf, H. and Zsigmondy, R.** (1902). Uber sichtbarmachung und größenbestimmung ultramikoskopischer teilchen, mit besonderer anwendung auf goldrubingläser, *Annalen der Physik*, *315*(1), 1–39.

[8] **Schuman, J.S.**, **Wollstein, G.**, **Farra, T.**, **Hertzmark, E.**, **Aydin, A.**, **Fujimoto, J.G. and Paunescu, L.A.** (2003). Comparison of optic nerve head measurements obtained by optical coherence tomography and confocal scanning laser ophthalmoscopy, *American journal of ophthalmology*, *135*(4), 504–512.

[9] **Jemielita, M.**, **Taormina, M.J.**, **DeLaurier, A.**, **Kimmel, C.B. and Parthasarathy, R.** (2013). Comparing phototoxicity during the development of a zebrafish craniofacial bone using confocal and light sheet fluorescence microscopy techniques, *Journal of biophotonics*, *6*(11-12), 920–928.

[10] **Gu, M. and Sheppard, C.** (1995). Comparison of three-dimensional imaging properties between two-photon and single-photon fluorescence microscopy, *Journal of microscopy*, *177*(2), 128–137.

[11] **Duan, Y. and Chen, N.** (2015). Hybrid wide-field and scanning microscopy for high-speed 3D imaging, *Optics letters*, *40*(22), 5251–5254.

[12] **Podoleanu, A.G.**, **Dobre, G.M.**, **Cucu, R.G.**, **Rosen, R.B.**, **Garcia, P.**, **Nieto, J.**, **Will, D.V.**, **Gentile, R.C.**, **Muldoon, T.**, **Walsh, J.B.**

et al. (2004). Combined multiplanar optical coherence tomography and confocal scanning ophthalmoscopy, *Journal of biomedical optics*, *9*(1), 86–94.

[13] **Beaurepaire, E.**, **Moreaux, L.**, **Amblard, F. and Mertz, J.** (1999). Combined scanning optical coherence and two-photon-excited fluorescence microscopy, *Optics Letters*, *24*(14), 969–971.

[14] **Chen, Y.**, **Liang, C.P.**, **Liu, Y.**, **Fischer, A.H.**, **Parwani, A.V. and Pantanowitz, L.** (2012). Review of advanced imaging techniques, *Journal of pathology informatics*, *3*.

[15] **Jonkman, J. and Brown, C.M.** (2015). Any way you slice it—a comparison of confocal microscopy techniques, *Journal of biomolecular techniques: JBT*, *26*(2), 54.

[16] **Qiu, Z. and Piyawattanametha, W.** (2015). MEMS based fiber optical microendoscopes, *Displays*, *37*, 41–53.

[17] **Conchello, J.A. and Lichtman, J.W.** (2005). Optical sectioning microscopy, *Nature methods*, *2*(12), 920–931.

[18] **Helmchen, F. and Denk, W.** (2005). Deep tissue two-photon microscopy, *Nature methods*, *2*(12), 932–940.

[19] **Neerken, S.**, **Lucassen, G.W.**, **Nuijs, T.A.M.**, **Lenderink, E. and Hendriks, R.F.M.**, (2004). Comparison of Confocal Laser Scanning Microscopy and Optical Coherence Tomography, Springer US, New York, NY, pp.949–971, `https://doi.org/10.1007/0-387-29989-0_22`.

[20] **Durnin, J.**, **Miceli Jr, J. and Eberly, J.** (1987). Diffraction-free beams, *Physical review letters*, *58*(15), 1499.

[21] **Durnin, J.** (1987). Exact solutions for nondiffracting beams. I. The scalar theory, *JOSA A*, *4*(4), 651–654.

[22] **Chattrapiban, N.**, **Rogers, E.A.**, **Cofield, D.**, **Hill III, W.T. and Roy, R.** (2003). Generation of nondiffracting Bessel beams by use of a spatial light modulator, *Optics letters*, *28*(22), 2183–2185.

[23] **Choi, Y.**, **Yoon, C.**, **Kim, M.**, **Yang, T.D.**, **Fang-Yen, C.**, **Dasari, R.R.**, **Lee, K.J. and Choi, W.** (2012). Scanner-free and wide-field endoscopic imaging by using a single multimode optical fiber, *Physical review letters*, *109*(20), 203901.

[24] **Zhu, X.**, **Schülzgen, A.**, **Li, L. and Peyghambarian, N.** (2009). Generation of controllable nondiffracting beams using multimode optical fibers, *Applied physics letters*, *94*(20), 201102.

[25] **Zhu, X.**, **Schülzgen, A.**, **Wei, H.**, **Kieu, K. and Peyghambarian, N.** (2011). White light Bessel-like beams generated by miniature all-fiber device, *Optics express*, *19*(12), 11365–11374.

[26] **Bouchal, Z.**, **Wagner, J. and Chlup, M.** (1998). Self-reconstruction of a distorted nondiffracting beam, *Optics Communications*, *151*(4-6), 207–211.

[27] **Fahrbach, F.O.**, **Simon, P. and Rohrbach, A.** (2010). Microscopy with self-reconstructing beams, *Nature photonics*, *4*(11), 780.

[28] **Chen, Y. and Liu, J.T.** (2015). Characterizing the beam steering and distortion of Gaussian and Bessel beams focused in tissues with microscopic heterogeneities, *Biomedical optics express*, *6*(4), 1318–1330.

[29] **Gori, F.**, **Guattari, G. and Padovani, C.** (1987). Bessel-gauss beams, *Optics communications*, *64*(6), 491–495.

[30] **Thibon, L.**, **Lorenzo, L.E.**, **Piché, M. and De Koninck, Y.** (2017). Resolution enhancement in confocal microscopy using Bessel-Gauss beams, *Optics express*, *25*(3), 2162–2177.

[31] **Lee, K.S. and Rolland, J.P.** (2008). Bessel beam spectral-domain high-resolution optical coherence tomography with micro-optic axicon providing extended focusing range, *Optics letters*, *33*(15), 1696–1698.

[32] **Leitgeb, R.**, **Villiger, M.**, **Bachmann, A.**, **Steinmann, L. and Lasser, T.** (2006). Extended focus depth for Fourier domain optical coherence microscopy, *Optics letters*, *31*(16), 2450–2452.

[33] **Gao, L.**, **Shao, L.**, **Chen, B.C. and Betzig, E.** (2014). 3D live fluorescence imaging of cellular dynamics using Bessel beam plane illumination microscopy, *Nature protocols*, *9*(5), 1083.

[34] **Fahrbach, F.O.**, **Simon, P. and Rohrbach, A.** (2010). Microscopy with self-reconstructing beams, *Nature photonics*, *4*(11), 780.

[35] **Curatolo, A.**, **Munro, P.R.**, **Lorenser, D.**, **Sreekumar, P.**, **Singe, C.C.**, **Kennedy, B.F. and Sampson, D.D.** (2016). Quantifying the influence of Bessel beams on image quality in optical coherence tomography, *Scientific reports*, *6*, 23483.

[36] **Borglin, J.**, **Wang, D.**, **Durr, N.J.**, **Hanstorp, D.**, **Ben-Yakar, A. and Ericson, M.B.** (2017). Annular Beam Shaping in Multiphoton Microscopy to Reduce Out-of-Focus Background, *International Journal of Spectroscopy*, *2017*.

[37] **Antonacci, G.**, **Di Domenico, G.**, **Silvestri, S.**, **DelRe, E. and Ruocco, G.** (2017). Diffraction-free light droplets for axially-resolved volume imaging, *Scientific reports*, *7*(1), 1–6.

[38] **Di Domenico, G.**, **Ruocco, G.**, **Colosi, C.**, **DelRe, E. and Antonacci, G.** (2018). Cancellation of Bessel beam side lobes for high-contrast light sheet microscopy, *Scientific reports*, *8*(1), 1–7.

[39] **Fahrbach, F.O.**, **Gurchenkov, V.**, **Alessandri, K.**, **Nassoy, P. and Rohrbach, A.** (2013). Self-reconstructing sectioned Bessel beams offer submicron optical sectioning for large fields of view in light-sheet microscopy, *Optics express*, *21*(9), 11425–11440.

[40] **Jia, H.**, **Yu, X.**, **Yang, Y.**, **Zhou, X.**, **Yan, S.**, **Liu, C.**, **Lei, M. and Yao, B.** (2019). Axial resolution enhancement of light-sheet microscopy by double scanning of Bessel beam and its complementary beam, *Journal of biophotonics*, *12*(1), e201800094.

[41] **Silvestri, L.**, **Bria, A.**, **Sacconi, L.**, **Iannello, G. and Pavone, F.** (2012). Confocal light sheet microscopy: micron-scale neuroanatomy of the entire mouse brain, *Optics express*, *20*(18), 20582–20598.

[42] **Fahrbach, F.O. and Rohrbach, A.** (2012). Propagation stability of self-reconstructing Bessel beams enables contrast-enhanced imaging in thick media, *Nature communications*, *3*(1), 1–8.

[43] **Yang, Z.**, **Mei, L.**, **Xia, F.**, **Luo, Q.**, **Fu, L. and Gong, H.** (2015). Dual-slit confocal light sheet microscopy for in vivo whole-brain imaging of zebrafish, *Biomedical optics express*, *6*(5), 1797–1811.

[44] **Planchon, T.A.**, **Gao, L.**, **Milkie, D.E.**, **Davidson, M.W.**, **Galbraith, J.A.**, **Galbraith, C.G. and Betzig, E.** (2011). Rapid three-dimensional isotropic imaging of living cells using Bessel beam plane illumination, *Nature methods*, *8*(5), 417.

[45] **Fahrbach, F.O.**, **Gurchenkov, V.**, **Alessandri, K.**, **Nassoy, P. and Rohrbach, A.** (2013). Light-sheet microscopy in thick media using scanned Bessel beams and two-photon fluorescence excitation, *Optics express*, *21*(11), 13824–13839.

[46] **Thériault, G.**, **De Koninck, Y. and McCarthy, N.** (2013). Extended depth of field microscopy for rapid volumetric two-photon imaging, *Optics express*, *21*(8), 10095–10104.

[47] **Thériault, G.**, **Cottet, M.**, **Castonguay, A.**, **McCarthy, N. and De Koninck, Y.** (2014). Extended two-photon microscopy in live samples with Bessel beams: steadier focus, faster volume scans, and simpler stereoscopic imaging, *Frontiers in cellular neuroscience*, *8*, 139.

[48] **Borglin, J.**, **Wang, D.**, **Durr, N.J.**, **Hanstorp, D.**, **Ben-Yakar, A. and Ericson, M.B.** (2017). Annular Beam Shaping in Multiphoton Microscopy to Reduce Out-of-Focus Background, *International Journal of Spectroscopy*, *2017*.

[49] **Fahrbach, F.O.**, **Simon, P. and Rohrbach, A.** (2010). Microscopy with self-reconstructing beams, *Nature Photonics*, *4*(11), 780.

[50] **Murshid, S.**, **Grossman, B. and Narakorn, P.** (2008). Spatial domain multiplexing: A new dimension in fiber optic multiplexing, *Optics & Laser Technology*, *40*(8), 1030–1036.

[51] **Khayatzadeh, R.**, **Çivitci, F. and Ferhanoğlu, O.** (2017). Optimization of piezo-fiber scanning architecture for low voltage/high displacement operation, *Sensors and Actuators A: Physical*, *255*, 21–27.

[52] **Lee, C.M.**, **Engelbrecht, C.J.**, **Soper, T.D.**, **Helmchen, F. and Seibel, E.J.** (2010). Scanning fiber endoscopy with highly flexible, 1 mm catheterscopes for wide-field, full-color imaging, *Journal of biophotonics*, *3*(5-6), 385–407.

[53] **Yildirim, M.**, **Ferhanoglu, O.**, **Kobler, J.B.**, **Zeitels, S.M. and Ben-Yakar, A.** (2013). Parameters affecting ultrafast laser microsurgery of subepithelial voids for scar treatment in vocal folds, *Journal of biomedical optics*, *18*(11), 118001.

[54] **Seibel, E.J. and Smithwick, Q.Y.** (2002). Unique features of optical scanning, single fiber endoscopy, *Lasers in Surgery and Medicine: The Official Journal of the American Society for Laser Medicine and Surgery*, *30*(3), 177–183.

[55] **Hoy, C.L.**, **Durr, N.J. and Ben-Yakar, A.** (2011). Fast-updating and nonrepeating Lissajous image reconstruction method for capturing increased dynamic information, *Applied optics*, *50*(16), 2376–2382.

[56] **Teo, Y.R.**, **Yong, Y. and Fleming, A.J.** (2018). A comparison of scanning methods and the vertical control implications for scanning probe microscopy, *Asian Journal of Control*, *20*(4), 1352–1366.

[57] **Rivera, D.R.**, **Brown, C.M.**, **Ouzounov, D.G.**, **Pavlova, I.**, **Kobat, D.**, **Webb, W.W. and Xu, C.** (2011). Compact and flexible raster scanning multiphoton endoscope capable of imaging unstained tissue, *Proceedings of the National Academy of Sciences*.

[58] **Khayatzadeh, R.**, **Ferhanoğlu, O. and Çivitci, F.** (2017). Unwarped Lissajous Scanning with Polarization Maintaining Fibers, *IEEE Photonics Technology Letters*, *29*(19), 1623–1626.

[59] **Jakobsen, J.** (2001). Danish guidelines on environmental low frequency noise, infrasound and vibration, *Journal of Low Frequency Noise, Vibration and Active Control*, *20*(3), 141–148.

[60] **Hwang, K.**, **Seo, Y.H.**, **Ahn, J.**, **Kim, P. and Jeong, K.H.** (2017). Frequency selection rule for high definition and high frame rate Lissajous scanning, *Scientific reports*, *7*(1), 14075.

[61] **Le Harzic, R.**, **Weinigel, M.**, **Riemann, I.**, **König, K. and Messerschmidt, B.** (2008). Nonlinear optical endoscope based on a compact two axes piezo scanner and a miniature objective lens, *Optics express*, *16*(25), 20588–20596.

[62] **Hwang, K.**, **Seo, Y.H.**, **Ahn, J.**, **Kim, P. and Jeong, K.H.** (2017). Frequency selection rule for high definition and high frame rate Lissajous scanning, *Scientific reports*, *7*(1), 14075.

[63] **Sullivan, S.Z.**, **Muir, R.D.**, **Newman, J.A.**, **Carlsen, M.S.**, **Sreehari, S.**, **Doerge, C.**, **Begue, N.J.**, **Everly, R.M.**, **Bouman, C.A. and Simpson, G.J.** (2014). High frame-rate multichannel beam-scanning microscopy based on Lissajous trajectories, *Optics express*, *22*(20), 24224–24234.

CURRICULUM VITAE

Name Surname: Miyase Tekpınar

Place and Date of Birth: Konya, 05.11.1994

E-Mail: tekpinar@itu.edu.tr

EDUCATION:

- **B.Sc.:** 2017, Istanbul Technical University, Electric and Electronics Engineering Faculty, Electronics and Communication Engineering

PROFESSIONAL EXPERIENCE:

- 2018 Research Assistant at Istanbul Technical University

PUBLICATIONS ON THE THESIS:

- M. Tekpinar and O. Ferhanoglu, Synchronous Imaging of Multiple Slices with Single Lateral Scan using Higher-Order Bessel Beams and a Spherical Lens, Submitted to Photonics Technology Letters in January 2020.
- M. Tekpınar, R. Khayatzadeh and O. Ferhanoğlu, Multiple-pattern generating piezoelectric fiber scanner toward endoscopic applications. Optical Engineering, 58 (2019), 023101.